Diagn Interv Radiol 2016; 22:301–307

ABDOMINAL IMAGING

ORIGINAL ARTICLE

Feasibility of histogram analysis of susceptibility-weighted MRI for staging of liver fibrosis

Zhao-Xia Yang
He-Yue Liang
Xin-Xing Hu
Ya-Qin Huang
Ying Ding
Shan Yang
Meng-Su Zeng
Sheng-Xiang Rao

PURPOSE
We aimed to evaluate whether histogram analysis of susceptibility-weighted imaging (SWI) could quantify liver fibrosis grade in patients with chronic liver disease (CLD).

METHODS
Fifty-three patients with CLD who underwent multi-echo SWI (TEs of 2.5, 5, and 10 ms) were included. Histogram analysis of SWI images were performed and mean, variance, skewness, kurtosis, and the 1st, 10th, 50th, 90th, and 99th percentiles were derived. Quantitative histogram parameters were compared. For significant parameters, further receiver operating characteristic (ROC) analyses were performed to evaluate the potential diagnostic performance for differentiating liver fibrosis stages.

RESULTS
The number of patients in each pathologic fibrosis grade was 7, 3, 5, 5, and 33 for F0, F1, F2, F3, and F4, respectively. The results of variance (TE: 10 ms), 90th percentile (TE: 10 ms), and 99th percentile (TE: 10 and 5 ms) in F0–F3 group were significantly lower than in F4 group, with areas under the ROC curves (AUCs) of 0.84 for variance and 0.70–0.73 for the 90th and 99th percentiles, respectively. The results of variance (TE: 10 and 5 ms), 99th percentile (TE: 10 ms), and skewness (TE: 2.5 and 5 ms) in F0–F2 group were smaller than those of F3/F4 group, with AUCs of 0.88 and 0.69 for variance (TE: 10 and 5 ms, respectively), 0.68 for 99th percentile (TE: 10 ms), and 0.73 and 0.68 for skewness (TE: 2.5 and 5 ms, respectively).

CONCLUSION
Magnetic resonance histogram analysis of SWI, particularly the variance, is promising for predicting advanced liver fibrosis and cirrhosis.

Liver fibrosis is the accumulation of extracellular matrix proteins and is a feature of most chronic liver diseases (CLDs) (1). Studies have demonstrated that fibrosis is reversible at early stages (2, 3), and causal treatments improve liver function (4). Because of the great risk of liver cirrhosis, hepatocellular carcinoma (HCC), and other complications in patients with liver fibrosis, accurate assessment of the liver fibrosis stage and early detection of early cirrhosis are important for judging the prognosis and planning treatment (5). Furthermore, the severity of fibrosis has been associated with remnant liver functional reserve after hepatectomy for HCC (6). A noninvasive tool that would enable us to preoperatively evaluate the severity of liver fibrosis would be beneficial for a more risk-adapted treatment strategy.

Liver biopsy is commonly considered to be the gold standard for grading liver fibrosis; however, biopsy is considered impractical for evaluating disease progression or response to treatment because of its invasiveness, interobserver variability, sample errors, patients' acceptance, and complications such as bleeding, infection, and pain (7–10). Consequently, a noninvasive and feasible method for assessing the liver fibrosis stage is required. Conventional axial imaging techniques have limited value for evaluating liver fibrosis. Recently, several noninvasive methods have been assessed, including laboratory tests, ultrasound transient elastography (11), and magnetic resonance imaging (MRI)-based techniques (e.g., magnetic elastography, diffusion-weighted imaging [DWI], perfusion, gadoxetic acid-enhanced MRI, and susceptibility-weighted imaging [SWI]) (12–21). SWI was demonstrated to be feasible for abdominal imaging and could utilize phase information to enhance susceptibility effects that were caused by iron in cirrhosis and HCC

From the Department of Radiology (S.X.R. ✉ *raoxray@163.com*), Zhongshan Hospital of Fudan University and Shanghai Institute of Medical Imaging, Shanghai, China.

Received 1 July 2015; revision requested 28 July 2015; last revision received 6 November 2015; accepted 10 November 2015.

Published online 25 April 2016.
DOI 10.5152/dir.2016.15284

(22, 23). In theory, increased iron content of the liver and secondary changes manifesting in progressive collagen deposition are important background alterations in the development of liver fibrosis (24). Balassy et al. (21) reported that by measuring the mean values of signal intensities and using a corrected liver-to-muscle ratio, SWI might be used as an alternative technique to assess the severity of hepatic fibrosis. However, they did not consider the heterogeneity of fibrotic liver parenchyma.

Image texture is a sensitive characteristic for assessing pathology, and texture analysis is a method that can provide more information regarding the image texture features that may be ignored by visual evaluation (25). A histogram is a useful tool in hepatic texture analysis for depicting the distribution of signal intensity levels (26), which can reflect the heterogeneity of pathologic changes. Kim et al. (27) demonstrated that histogram analysis of gadoxetic acid-enhanced hepatobiliary phase MRI could be useful in depicting enhancement heterogeneity, which is representative of the liver fibrosis stage (27). We hypothesized that the fibrotic liver had different heterogeneities of iron deposition and secondary changes in different fibrosis stages, which might be detected by histogram analyses of SWI.

Thus, we aimed to evaluate whether histogram analysis of SWI could quantify liver fibrosis stages and assess whether different echo times (TEs) of SWI could affect the quantification of SWI histogram analyses.

Main points

- Accurate assessment of fibrosis stage using a noninvasive method is important in clinical practice.
- Histogram analysis reveals the distribution of signal intensity levels for susceptibility-weighted images and has the potential to detect different heterogeneity of iron deposition and secondary changes of liver parenchyma in different fibrosis stages.
- We identified histogram-derived parameters on susceptibity-weighted images (in particular, variance) as potentially useful biomarkers for predicting stages of liver fibrosis.
- In the present study, higher TE, especially TE=10 ms, was found to be more accurate for staging fibrosis compared with TE=2.5 ms or 5 ms.

Methods

Patients

We retrospectively evaluated 215 consecutive patients who were suspected to have CLDs or focal liver lesions clinically or through previous imaging by ultrasonography (US), computed tomography (CT), or MRI between March 2010 and May 2011. The Institutional Review Board of our hospital approved the study and waived informed consent. The inclusion criteria were as follows: histopathologically confirmed liver fibrosis stages with partial hepatectomy conducted to treat HCC; availability of preoperative MRI, including SWI sequence, obtained using the same 3.0 T MRI scanner; patients without prior partial hepatectomy or anticancer treatments (e.g., transarterial chemoembolization, radiofrequency ablation, or radiation therapy); and patients without systemic diseases or iron overload history that may have an effect on the liver (e.g., metabolic disorders, iron deficiency anemia, or repetitive blood transfusion). Finally, the defined sample comprised 53 patients with documented pathologic fibrosis stages (classified according to the METAVIR system). Serum alpha fetoprotein (AFP), alanine aminotransferase, aspartate aminotransferase, and bilirubin levels were obtained within two weeks before MRI was performed.

MRI acquisition

All patients were imaged at a 3.0 T MRI scanner (Verios, Siemens) using a 12-channel body coil. The following MRI sequences were used: T2-weighted fast-spin echo sequence (TR/TE, 4000/78 ms), with fat suppression, lateral respiratory navigation, and a flip angle of 140°; T1-weighted with fast low-angle (70°) shot sequence (TR/TE, 140/2.5 ms); section thickness was 5 mm, intersection gap was 1 mm; and matrix was 168–180×320. For dynamic contrast imaging, gadopentetate dimeglumine (Magnevist, Bayer Healthcare) was injected after a 20 mL saline flush (Spectris, Medrad); the parameters for dynamic contrast were TR/TE, 4/1.4 ms; matrix, 180×320; flip angle, 9°; and section thickness, 3 mm, and there was no intersection gap. Hepatic arterial, portal, and equilibrium phase images were obtained at 25, 60, and 180 s after contrast-median administration, respectively. For the transverse muti-echo two-dimensional SWI sequence that was performed before the enhancement, the parameters were TR/TEs, 150/10, 5, and 2.5 ms; matrix, 187×384; flip angle, 20°; voxel size, 1.5×1.0×0.5 mm^3; section thickness, 5 mm; and intersection gap, 1 mm. FOV of all sequences was the same (285×214 to 285×380 mm). For covering the entire liver, we used three breath holds; each of these lasted for 16 s, and 30 slices were used. Total time of breath holds was <77 s for all patients, including break time between multiple breath holds. A corresponding imaging technology, generalized autocalibrating partially parallel acquision, was used with an acceleration factor of 2. Once SWI was performed, the images (phases, magnitudes, SWI images, and minimum intensity projections) were re-established on the MRI console.

Histogram analysis

The SWI images were transferred from the hospital's picture archiving and communication system to an offline workstation. Histogram analyses were performed using MaZda (MaZda for Windows, B11 version 3.3, www.eletel.p.lodz.pl/programy/mazda/) (28, 29). Two abdominal radiologists, with one year (Y.Z.X.) and two years (L.H.Y.) of abdominal imaging experience, who were blinded to the clinical information and liver fibrosis stages, placed regions of interest (ROI) of the liver parenchyma at the portal hepatic level, thus avoiding visible abnormalities (tumors, cysts, hemangiomas, etc.) and visible veins and bile ducts for each patient (Fig. 1). When the abnormalities were small and could be easily ignored on the SWI images, T1- and T2-weighted images were also reviewed. Once ROI was placed, gray-level normalization was performed for each ROI, and the limitation of dynamics to $\mu\pm3\sigma$ (μ, gray-level mean and σ, gray-level standard deviation) was used to decrease the influence of variations in contrast and brightness. Histogram data was then generated for ROI, and the following parameters were calculated: mean, variance, skewness, kurtosis, and the 1st, 10th, 50th, 90th, and 99th percentiles. These parameters are mathematically defined below.

Mean, $\mu=\sum_{i=1}^{Ng} ip(i)$;

Variance, $\sigma^2=\sum_{i=1}^{Ng}(i-\mu)^2 p(i)$;

Skewness, $\mu_3=\sigma^{-3}\sum_{i=1}^{Ng}(i-\mu)^3 p(i)$;

Kurtosis, $\mu_4=\sigma^{-4}\sum_{i=1}^{Ng}(i-\mu)^4 p(i)-3$;

n^{th} percentile means the point at which n% of the voxel values that form the histogram are found to the left. In the formulas, p(i) is a normalized histogram vector (i.e., a histogram whose entries are divided by the sum

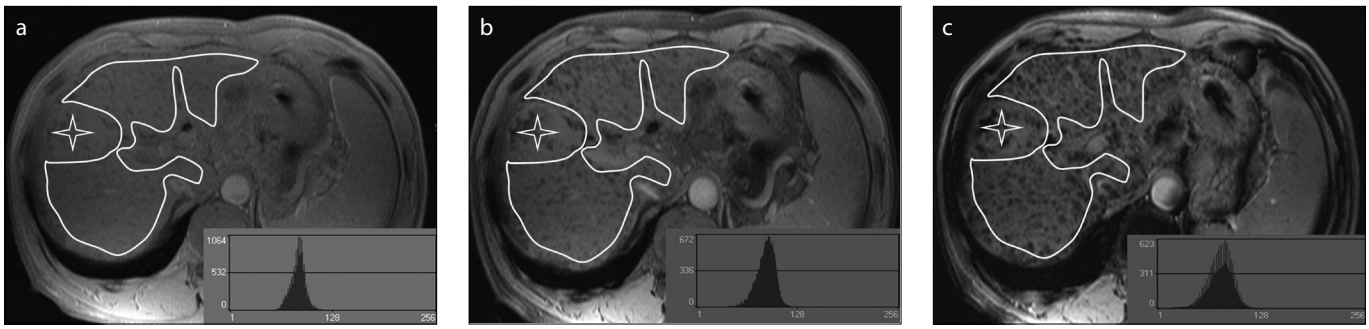

Figure 1. a–c. Examples of regions of interest drawn over susceptibility-weighted images of the liver. Liver borders, visible lesions *(asterisk)*, major vessels, and vena cava were manually excluded. Images represent the different echo time (TE) values: **(a)**, TE=2.5 ms; **(b)**, TE=5 ms; **(c)**, TE=10 ms. The histogram curves are shown on the bottom left.

Table 1. Statistics of susceptibility-weighted MRI histogram analysis parameters measured for hepatic parenchyma at different TE values between F0–F3 group (noncirrhotic liver) and F4 group (cirrhotic liver)

	TE=2.5 ms			TE=5.0 ms			TE=10 ms		
	F0–F3 (n=20)	F4 (n=33)	*P*	F0–F3 (n=20)	F4 (n=33)	*P*	F0–F3 (n=20)	F4 (n=33)	*P*
Mean	78.3 (66.2, 115.4)	81.3 (67.1, 102.4)	0.463	82.1 (62.5, 120.3)	86.7 (65.8, 104.3)	0.359	69.2 (41.5, 109.6)	78.0 (43.9, 103.0)	0.091
Variance	120.5 (42.8, 257.7)	135.8 (65.2, 451.2)	0.557	139.8 (51.4, 429.1)	154.0 (69.7, 525.2)	0.106	106.8 (55.8, 174.9)	157.5 (94.0, 512.3)	0.000*
Skewness	0.2 (–0.3, 0.9)	0.4 (–0.2, 1.1)	0.287	0.2 (–0.4, 0.9)	0.3 (–0.4, 0.8)	0.137	0.4 (–0.3, 1.4)	0.3 (–0.4, 1.5)	0.557
Kurtosis	–0.1 (–0.7, 1.7)	–0.3 (–1.0, 1.2)	0.927	–0.3 (–0.7, 0.8)	0.03 (–1.0, 1.0)	0.369	0.4 (–0.6, 2.7)	0.2 (–0.8, 6.0)	0.255
1st percentile	59.3±15.5	60.1±10.4	0.818	60.1±15.7	60.2±10.2	0.987	51.7±17.0	50.9±12.2	0.856
10th percentile	67.1±15.1	67.5±10.2	0.914	69.5±15.7	70.2±9.9	0.857	59.6±17.6	62.2±12.4	0.539
50th percentile	82.5 (65, 115.5)	79.0 (66.0, 101.5)	0.576	80.8 (62.0, 121.0)	86.0 (64.0, 104.5)	0.452	68.3 (40.5, 110.0)	77.0 (42.0, 101.5)	0.114
90th percentile	95.9±11.8	98.9±9.3	0.320	100.4±13.4	105.1±9.2	0.140	85.6±17.8	97.1±12.4	0.017*
99th percentile	108.2±12.6	112.1±11.3	0.247	112.4±13.4	119.9±11.4	0.035*	98.9±16.5	112.5±13.5	0.002*

Data are presented as mean±standard deviation for normal distribution or median (minimum, maximum) for non-normal distribution.
TE, echo time.
*$P < 0.05$.

of the pixels in ROI), i=1, 2, …, and Ng means the number of intensity levels.

Standard reference

All patients underwent a partial hepatectomy for resection of HCC. The surrounding hepatic parenchyma was also excised to diagnose the underlying liver disease. All surgical specimens were assessed by a dedicated pathologist with 10 years of experience, who was blinded to radiologic analyses. The criteria for liver fibrosis stages were as follows: F0, no fibrosis; F1, fibrous expansion of some portal areas; F2, bridging fibrosis; F3, fibrosis septa with architectural distortion; and F4, cirrhosis.

Statistical analysis

A comparison of mean, variance, skewness, kurtosis, and the 1st, 10th, 50th, 90th, and 99th percentiles of the groups were calculated using the Student's *t*-test or Mann-Whitney U test. For the calculations of parameters previously described, each parameter was averaged between the two readers. Interobserver agreement was assessed by calculating the intraclass correlation coefficient (ICC) for single measurements. For significant parameters, receiver operating characteristics (ROC) analyses were further established to evaluate the potential diagnostic performance for differentiating liver fibrosis stages. Corresponding areas under the ROC curve (AUCs) with 95% confidence intervals (CI) were calculated. The optimal cutoff values of the value histogram analysis parameters for distinguishing F0–F2 group (no liver fibrosis to moderate liver fibrosis) and F3/F4 group (advanced liver fibrosis) and F0–F3 group (noncirrhotic liver) and F4 group (cirrhotic liver) were calculated to maximize the sum of specificity and sensitivity; we selected the cutoff value at which the Youden index was the maximum value. The analyses were performed using the SPSS software (19.0, IBM Corp.) and MedCalc (MedCalc for Windows, ver. 11.5.0.0, www.medcalc.be). A *P* value of <0.05 was considered significant.

Results

In the study, 43 patients were male and 10 were female. Their mean age was 51.9±11.7 years, ranging from 25 to 75 years. Among these, only one patient did not suffer from an identifiable underlying CLD; all others had viral hepatitis B, and pathologic results demonstrated that all had HCC. MRI was completed before hepatectomy within 20 days (5.8±4.5 days; range, 1–20 days). The number of patients in each pathologic fibrosis grade was 7, 3, 5, 5, and 33 for F0, F1, F2, F3, and F4, respectively. The median baseline AFP, bilirubin, aspartate aminotransferase, and alanine aminotransferase levels were 51.65 ng/mL (range, 0.70–7605.00 ng/mL), 11.80 µmol/L (range, 4.70–181.20 µmol/L), 32.00 U/L (range, 8.40–121.00 U/L), and 33.50 U/L (range, 13.00–128.00 U/L), respectively.

When TE was 2.5 or 5 ms for the above-mentioned parameters including mean, variance, skewness, the 1st, 10th, 50th, 90th, and 99th percentiles, interobserver agree-

Table 2. Statistics of susceptibility-weighted MRI histogram analysis parameters measured for hepatic parenchyma at different TE values between F0–F2 group (no liver fibrosis to moderate liver fibrosis) and F3/F4 group (advanced liver fibrosis)

	TE=2.5 ms			TE=5 ms			TE=10 ms		
	F0–F2 (n=15)	F3/F4 (n=38)	*P*	F0–F2 (n=15)	F3/F4 (n=38)	*P*	F0–F2 (n=15)	F3/F4 (n=38)	*P*
Mean	83.5±14.0	81.2±9.2	0.479	87.3±14.0	85.3±9.7	0.555	75.1±16.9	76.7±13.6	0.721
Variance	105.2 (42.8, 257.7)	140.9 (65.2, 451.2)	0.086	109.1 (51.4, 429.1)	155.1 (69.7, 525.2)	0.035*	102.5 (55.8, 147.5)	156.3 (85.7, 512.3)	0.000*
Skewness	0.1(−0.3, 0.8)	0.5 (−0.2, 1.1)	0.011*	0.1 (−0.4, 0.8)	0.3 (−0.4, 0.9)	0.042*	0.2 (−0.3, 0.8)	0.3 (−0.4, 1.5)	0.418
Kurtosis	−0.3 (−0.7, 0.7)	−0.2 (−1.0, 1.7)	0.364	−0.3 (−0.7, 0.8)	0.04 (−1.0, 1.0)	0.179	0.002 (−0.6, 2.7)	0.2 (−0.8, 6.0)	0.890
1st percentile	61.9±16.6	59.0±10.4	0.536	63.3±15.8	58.9±10.8	0.254	54.7±15.7	49.8±13.3	0.261
10th percentile	69.6±16.2	66.5±10.1	0.489	72.2±15.9	69.1±10.6	0.405	62.7±16.5	60.1±13.8	0.637
50th percentile	83.4±14.2	79.8±9.5	0.291	87.2±14.3	84.2±10.2	0.394	74.8±16.9	75.8±14.0	0.835
90th percentile	97.3±12.7	98.0±9.4	0.831	102.6±13.3	103.6±10.3	0.786	88.0±17.5	94.7±14.6	0.160
99th percentile	108.0±12.7	111.7±11.5	0.319	114.0±14.3	118.3±11.9	0.264	99.5±16.9	110.9±14.8	0.024*

Data are presented as mean±standard deviation for normal distribution or median (minimum, maximum) for non-normal distribution.
TE, echo time.
*$P < 0.05$.

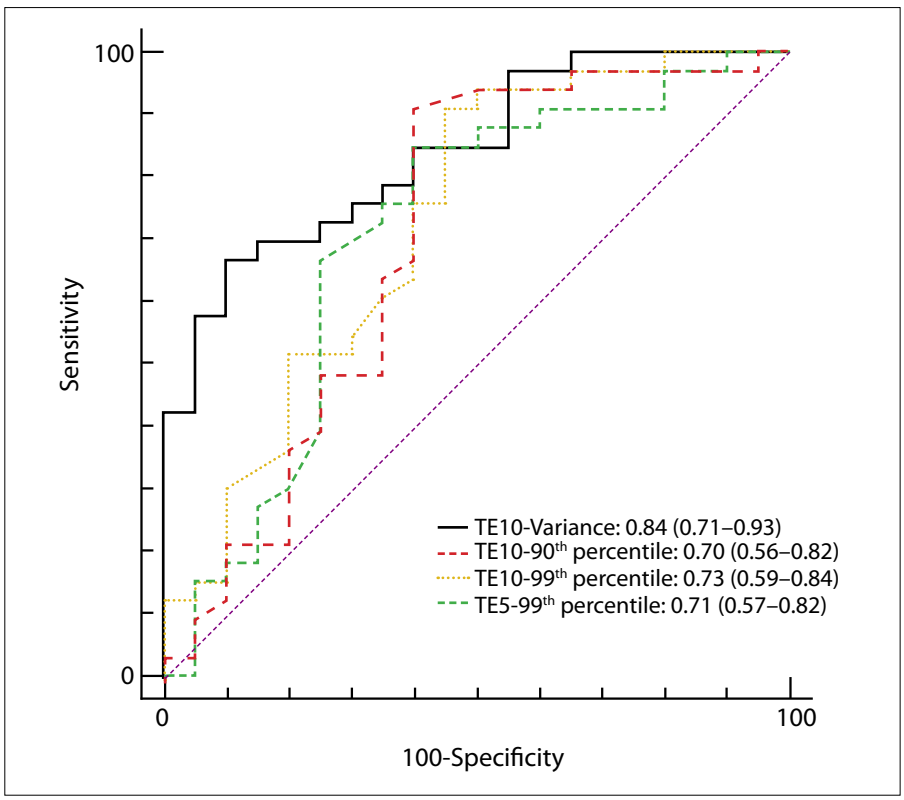

Figure 2. Receiver operating characteristics (ROC) analysis and areas under the curve (AUC) for prediction of liver cirrhosis (F4) by significant histogram parameters for susceptibility-weighted imaging (SWI). Numbers in parentheses represent 95% confidence interval (CI).

ment was excellent (ICC, 0.90–0.97) except for kurtosis (ICC, 0.74 and 0.63, respectively); when TE was 10 ms, interobserver agreement was good (ICC, 0.87–0.95). Furthermore, we applied the F test with a true value=0 to all ICCs, and *P* was < 0.001 for all.

SWI histogram analysis parameters of the different groups at different TE values are provided in Tables 1 and 2. For distinguishing F0–F3 group (noncirrhotic) from F4 group (cirrhotic), the variance value using TE=10 ms in F0–F3 was significantly lower in comparison with F4 ($P < 0.001$); meanwhile, when TE was 2.5 or 5 ms, the variance had no significant statistical difference ($P > 0.05$). The 90th and 99th percentile values were significantly lower for F0–F3 group than for F4 group using TE=10 ms (85.6 vs. 97.1, $P = 0.017$ for 90th percentile and 98.9 vs. 112.5, $P = 0.002$ for 99th percentile, respectively). Moreover, the 99th percentile values had significant differences at TE=5 ms (112.4 vs. 119.9, $P = 0.035$). For discriminating between F0–F2 and F3/F4 groups, the variance values at TE=10 and 5 ms in F0–F2 were significantly lower compared with F3/F4, respectively ($P < 0.001$ for TE=10 ms; $P = 0.035$ for TE=5 ms). The 99th percentile had significant differences at TE=10 ms (99.5 vs. 110.9, $P = 0.024$). The skewness values were also significantly smaller for F0–F2 group than for F3/F4 group using both TE=2.5 ms ($P = 0.011$) and TE=5 ms ($P = 0.042$). There were no significant differences in mean and kurtosis between F0–F3 and F4 (cirrhotic) groups or between F0–F2 and F3/F4 groups at all TE values.

For ROC analyses, the optimal cutoff values and the corresponding specificity, sensitivity, positive predictive value, and negative predictive value were calculated for distinguishing different groups (Tables 3, 4; Figs. 2, 3). AUCs of the abovementioned significant parameters for detecting the presence of cirrhotic liver (F4) were 0.84, 0.70, 0.73, and 0.71 for variance (TE=10 ms), 90th percentile (TE=10 ms), 99th percentile (TE=10 ms), and 99th percentile (TE=5 ms), respectively. Furthermore, for predicting advanced liver fibrosis (F3/F4), AUCs were 0.88, 0.68, 0.69, 0.68, and 0.73 for variance (TE=10 ms), 99th percentile (TE=10 ms), variance (TE=5 ms), skewness (TE=5 ms), and skewness (TE=2.5 ms), respectively.

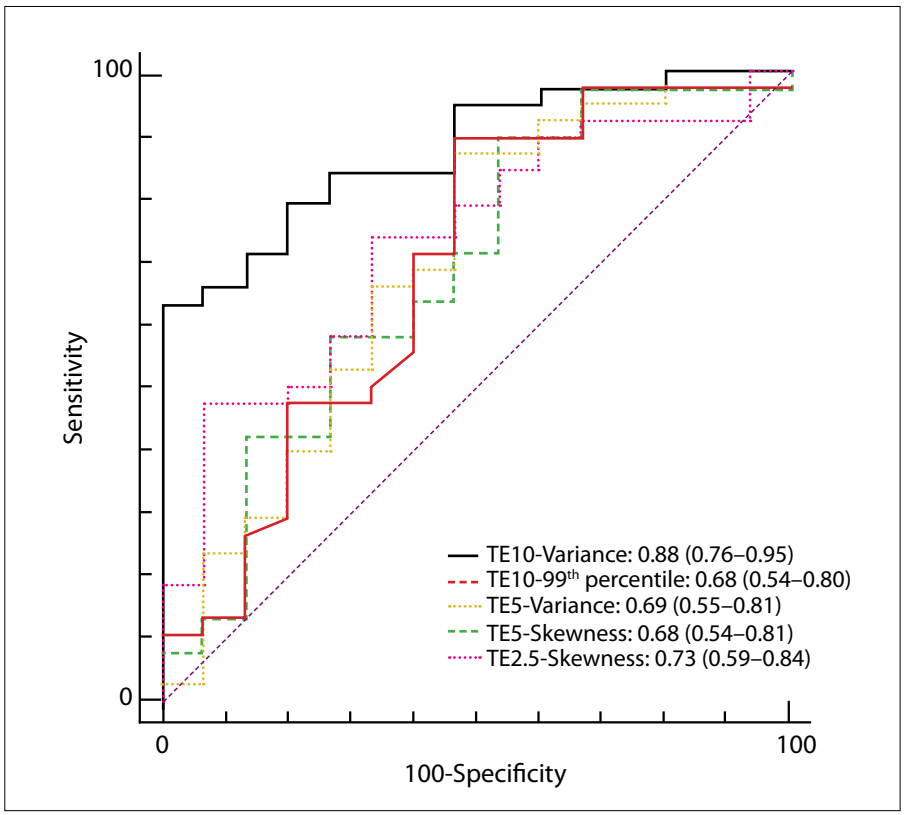

Figure 3. ROC analysis and AUC for prediction of advanced liver fibrosis (F3/F4) by significant histogram parameters for SWI. Numbers in parentheses represent 95% CI.

Table 3. Performance of the valuable parameters of susceptibility-weighted MRI histogram analyses at different TE values for identifying cirrhotic liver (F4)

TE	Parameters	AUC	*P**	Sensitivity	Specificity	PPV	NPV	Cutoff
10 ms	Variance	0.84	0.000	67	90	92	62	>147.4722
	95% CI	0.71–0.93		48–82	68–99	73–99	42–79	
	90th percentile	0.70	0.016	91	60	79	80	>84
	95% CI	0.56–0.82		76–98	36–81	62–91	52–95	
	99th percentile	0.73	0.003	91	55	77	79	>96
	95% CI	0.59–0.84		76–98	32–77	60–89	49–95	
5 ms	99th percentile	0.71	0.010	85	60	78	71	>111
	95% CI	0.57–0.82		68–95	36–81	61–90	44–90	

TE, echo time; AUC, area under the receiver operating characteristics curve; 95% CI, 95% confidence interval; PPV, positive predictive value; NPV, negative predictive value.
**P* value for AUC.

Discussion

This study aimed to explore the potential use of histogram analysis of muti-echo two-dimensional SWI for staging liver fibrosis in patients with CLD. The best results were obtained for histogram analysis of SWI (variance at TE=10 ms), with AUCs up to 0.84 for detecting cirrhotic liver and AUCs up to 0.88 for identifying advanced liver fibrosis, respectively. The 90th and 99th percentile could also be helpful to evaluate the liver fibrosis grade (AUCs, 0.68–0.73) when TE was 10 or 5 ms. Our study demonstrated that variance was the most valuable parameter for predicting the severity of liver fibrosis. Variance is a measure of the variation from the mean gray-level value and becomes greater when the image is more heterogeneous. This study demonstrated that a higher variance at TE=10 ms was found for cirrhotic liver compared with noncirrhotic liver, which was in keeping with the study by Nilsson et al. (30). Their study revealed that patients with cirrhosis were more nonhomogeneous compared with healthy controls. Furthermore, Kim et al. (27) reported that the correct coefficient of variation of histograms of the hepatobiliary phase of gadoxetic acid-enhanced MRI demonstrated statistically significant differences among different pathologic fibrosis grades (27). Our study also revealed that the variance of histograms in advanced liver fibrosis was greater for no liver fibrosis to moderate liver fibrosis, which might be because of the more nonhomogeneous iron deposition and secondary pathologic changes at higher grades of liver fibrosis. We also found that the histogram parameters of the 90th and 99th percentile could be useful in evaluating liver fibrosis grades. With the TE value being longer, the 90th and 99th percentile demonstrated a significant difference between different groups, particularly for the 99th percentile with higher AUC. The 99th percentile is a measure indicating the value below which 99% of the signal intensity within the study group falls, i.e., the maximum values of the histograms are excluded. These 1% maximum values may represent high signal intensity from artifacts that were incorrectly included in ROIs because of the limitations of manual ROI placement. Exclusion of these 1% maximum values may lead to SWI data that are more representative of the actual pathologic characteristics of the liver parenchyma itself. Compared with other parameters, these two parameters had relatively higher sensitivity, while the variance had greater specificity. It could be hypothesized that variance in combination with the 90th and 99th percentile measurements may be better for evaluating liver fibrosis; further study is required. In addition, we failed to demonstrate a benefit for low percentiles for grading liver fibrosis. Low signal intensity on SWI originates from the local magnetic susceptibility of substances such as iron. A possible explanation is that a low value represents the iron that exists in the different liver fibrosis stages. Based on our study, kurtosis did not provide valuable information for staging liver fibrosis, and the diagnostic performance of skewness (TE=2.5 or 5 ms) for identifying advanced liver fibrosis was relatively lower (AUC, 0.73 and 0.68, respectively). A previous study by Jira et al. (25) investigating texture analysis of T2-weighted imaging demonstrated positive results of

Table 4. Performance of the valuable parameters of susceptibility-weighted MRI histogram analyses at different TE values for identifying advanced liver fibrosis (F3/F4)

TE	Parameters	AUC	*P**	Sensitivity	Specificity	PPV	NPV	Cutoff
10 ms	Variance	0.88	0.000	63	100	100	52	>147.4722
	95% CI	0.76–0.95		46–78	78–100	86–100	32–71	
	99th percentile	0.68	0.047	89	53	83	67	>93
	95% CI	0.54–0.80		75–97	27–79	68–93	35–90	
5 ms	Variance	0.69	0.036	87	53	79	40	>109.0921
	95% CI	0.55–0.81		72–96	27–79	61–91	19–64	
	Skewness	0.68	0.042	63	60	80	39	>0.2068
	95% CI	0.54–0.81		46–78	32–84	61–92	20–61	
2.5 ms	Skewness	0.73	0.003	74	67	85	50	>0.1281
	95% CI	0.59–0.84		57–87	38–88	68–95	27–73	

TE, echo time; AUC, area under the receiver operating characteristics curve; 95% CI, 95% confidence interval; PPV, positive predictive value; NPV, negative predictive value.
**P* value for AUC.

kurtosis and skewness for assessing cirrhosis according to Child–Pugh scores; however, this study did not use histopathologic results as a standard reference. Conversely, we also realized that our dissatisfactory results for kurtosis and skewness might be because of sample errors for the small sample sizes of groups F0–F2 and the different sequences in our study. In addition, interobserver agreements of kurtosis were relatively low in our group.

In this study, we failed to demonstrate the benefits for grading liver fibrosis by the mean parameter of histogram analysis at all TE values. Contrary to our results, Balassy et al. (21) found that by measuring mean signal intensity, the liver-to-muscle ratio decreased with the progress of liver fibrosis and strongly correlated with liver fibrosis. This study aimed to assess the heterogeneity of liver parenchyma of the fibrosis by histogram analysis; therefore, we only calculated the direct mean signal intensity of the liver parenchyma and did not consider the muscle as reference. Furthermore, signal intensity is highly dependent on technical variations among SWI sequences generated by different MRI scanners. This might explain our poor results for mean parameter measurement compared with previous studies.

Recently, various TEs (2.5 or 10 ms) were applied for abdominal SWI to evaluate liver fibrosis and cirrhotic liver (21, 22, 31). In theory, susceptibility-weighted images acquired at a longer TE have a stronger susceptibility weighting and a lower image quality (32). At 1.5 T, SWI with a TE of 20 ms is equal to a TE of 10 ms at 3.0 T when considering susceptibility effects (22). In this study, higher TE, particularly with TE=10 ms, was found to be more accurate for staging fibrosis. The severity of liver fibrosis is associated with iron deposition (24) and images acquired at longer TE provided additional susceptibility contrast of iron-rich structures (32), resulting in the signal in the liver parenchyma with iron deposits becoming more evident by susceptibility contrast at longer TE. Studies demonstrated that SWI was the most sensitive imaging technique to detect siderotic nodules in cirrhotic liver compared with T1-, T2-, and T2*- weighted imaging when TE was 10 ms (22, 31).

Several new methods, such as FibroScan, DWI, perfusion, gadoxetic acid-enhanced MRI, and magnetic resonance elastography (11–20), are increasingly being used to assess liver fibrosis and have shown potential in predicting the severity of liver fibrosis. A previous multicenter prospective study showed that the diagnostic accuracy of FibroScan was high for cirrhosis but poor for significant fibrosis (F≥2) (11). However, DWI is less reliable because assessment of the apparent diffusion coefficient is confounded by fat and iron (33). Challenges in the state of perfusion MRI of the liver include the dual blood supplies of the liver, lack of uniform measurement, and breathing motion during the image acquisition. Gadoxetic acid-enhanced MRI should be used cautiously in patients with renal insufficiency, particularly in patients with a glomerular filtration rate of <30 mL/min/1.73 m^2 (34). While MRI is highly accurate and reliable in the diagnosis of fibrosis (12), it requires the use of expensive equipment, and considerable expertise. MRI histogram analysis is thus more beneficial than the above techniques, particularly because analyses can be performed based on routine SWI, and no additional scan time or contrast medium is required.

This study had several limitations. First, this was a retrospective study of prospectively acquired data; sampling bias was difficult to avoid, and the sample sizes for F0, F1, F2, and F3 were relatively small, which may have influenced the accuracy of SWI in grading liver fibrosis. Second, almost all the patients in our study had viral hepatitis B (only one had an uncertain underlying chronic disease), and all suffered hepatic carcinoma. Patients with other CLD should be explored. Third, we routinely performed the multi-echo SWI sequence using TEs=2.5/5/10 ms in clinical practice; therefore, the accuracy of histograms of SWI using TEs higher than 10 ms remains unknown, and needs further study. Fourth, we did not routinely measure liver iron content in pathologic evaluation in our hospital; therefore, we did not analyze the correlation between liver iron content and SWI values.

In conclusion, SWI histogram analysis holds promise to provide a noninvasive quantitative method for staging liver fibrosis in patients with CLDs. The histogram parameter of variance for SWI with TE=10 ms, which represents the heterogeneity of liver parenchyma, could be helpful for identifying advanced liver fibrosis or cirrhotic liver.

Conflict of interest disclosure

The authors declared no conflicts of interest.

References

1. Friedman SL. Liver fibrosis -- from bench to bedside. J Hepatol 2003; 38 (Suppl 1):S38–53. [CrossRef]
2. Friedman SL, Bansal MB. Reversal of hepatic fibrosis--fact or fantasy? Hepatology 2006; 43:S82–88. [CrossRef]
3. Fallowfield JA, Kendall TJ, Iredale JP. Reversal of fibrosis: no longer a pipe dream? Clin Liver Dis 2006; 10: 481–497. [CrossRef]
4. Popov Y, Schuppan D. Targeting liver fibrosis: strategies for development and validation of antifibrotic therapies. Hepatology 2009; 50:1294–1306. [CrossRef]
5. Motola DL, Caravan P, Chung RT, Fuchs BC. Noninvasive biomarkers of liver fibrosis: clinical applications and future directions. Curr Pathobiol Rep 2014; 2:245–256. [CrossRef]
6. Miyazaki S, Takasaki K, Yamamoto M, Tsugita M, Otsubo T. Liver regeneration and restoration of liver function after partial hepatectomy: the relation of fibrosis of the liver parenchyma. Hepatogastroenterology 1999; 46:2919–2924.
7. Rockey DC, Caldwell SH, Goodman ZD, Nelson RC, Smith AD. Liver biopsy. Hepatology 2009; 49:1017–1044. [CrossRef]

8. Myers RP, Fong A, Shaheen AA. Utilization rates, complications and costs of percutaneous liver biopsy: a population based study including 4275 biopsies. Liver Int 2008; 28:705–712. [CrossRef]
9. Terjung B, Lemnitzer I, Dumoulin FL, et al. Bleeding complications after percutaneous liver biopsy. An analysis of risk factors. Digestion 2003; 67:138–145. [CrossRef]
10. Bravo AA, Sheth SG, Chopra S. Liver biopsy. N Engl J Med 2001; 344:495–500. [CrossRef]
11. Degos F, Perez P, Roche B, et al. Diagnostic accuracy of FibroScan and comparison to liver fibrosis biomarkers in chronic viral hepatitis: a multicenter prospective study (the FIBROSTIC study). J Hepatol 2010; 53:1013–1021. [CrossRef]
12. Wang QB, Zhu H, Liu HL, Zhang B. Performance of magnetic resonance elastography and diffusion-weighted imaging for the staging of hepatic fibrosis: A meta-analysis. Hepatology 2012; 56:239–247. [CrossRef]
13. Bonekamp S, Torbenson MS, Kamel IR. Diffusion-weighted magnetic resonance imaging for the staging of liver fibrosis. J Clin Gastroenterol 2011; 45:885–892.[CrossRef]
14. Fujimoto K, Tonan T, Azuma S, et al. Evaluation of the mean and entropy of apparent diffusion coefficient values in chronic hepatitis C: correlation with pathologic fibrosis stage and inflammatory activity grade. Radiology 2011; 258:739–748. [CrossRef]
15. Do RK, Chandarana H, Felker E, et al. Diagnosis of liver fibrosis and cirrhosis with diffusion-weighted imaging: value of normalized apparent diffusion coefficient using the spleen as reference organ. AJR Am J Roentgenol 2010; 195:671–676. [CrossRef]
16. Hagiwara M, Rusinek H, Lee VS, et al. Advanced liver fibrosis: diagnosis with 3D whole-liver perfusion MR imaging-initial experience. Radiology 2008; 246:926–934. [CrossRef]
17. Nishie A, Asayama Y, Ishigami K, et al. MR prediction of liver fibrosis using a liver-specific contrast agent: super paramagnetic iron oxide versus Gd-EOB-DTPA. J Magn Reson Imaging 2012; 36:664–671. [CrossRef]
18. Watanabe H, Kanematsu M, Goshima S, et al. Staging hepatic fibrosis: comparison of gadoxetate disodium-enhanced and diffusion-weighted MR imaging--preliminary observations. Radiology 2011; 259:142–150. [CrossRef]
19. Goshima S, Kanematsu M, Watanabe H, et al. Gd-EOB-DTPA-enhanced MR imaging: prediction of hepatic fibrosis stages using liver contrast enhancement index and liver-to-spleen volumetric ratio. J Magn Reson Imaging 2012; 36:1148–1153. [CrossRef]
20. Choi YR, Lee JM, Yoon JH, Han JK, Choi BI. Comparison of magnetic resonance elastography and gadoxetate disodium-enhanced magnetic resonance imaging for the evaluation of hepatic fibrosis. Invest Radiol 2013; 48:607–613. [CrossRef]
21. Balassy C, Feier D, Peck-Radosavljevic M, et al. Susceptibility-weighted MR imaging in the grading of liver fibrosis: a feasibility study. Radiology 2014; 270:149–158. [CrossRef]
22. Chen W, DelProposto Z, Wu D, et al. Improved siderotic nodule detection in cirrhosis with susceptibility-weighted magnetic resonance imaging: a prospective study. PLoS One 2012; 7:e36454. [CrossRef]
23. Li RK, Zeng MS, Rao SX, et al. Using a 2D multibreath-hold susceptibility-weighted imaging to visualize intratumoral hemorrhage of hepatocellular carcinoma at 3T MRI: correlation with pathology. J Magn Reson Imaging 2012; 36:900–906. [CrossRef]
24. Schmeltzer PA, Talwalkar JA. Noninvasive tools to assess hepatic fibrosis: ready for prime time? Gastroenterol Clin North Am 2011; 40:507–521. [CrossRef]
25. Jirák D, Dezortová M, Taimr P, Hájek M. Texture analysis of human liver. J Magn Reson Imaging 2002; 15:68–74. [CrossRef]
26. Maeda K, Utsu M, Kihaile PE. Quantification of sonographic echogenicity with grey-level histogram width: a clinical tissue characterization. Ultrasound Med Biol 1998; 24:225–234. [CrossRef]
27. Kim H, Park SH, Kim EK, et al. Histogram analysis of gadoxetic acid-enhanced MRI for quantitative hepatic fibrosis measurement. PLoS One 2014; 9:e114224. [CrossRef]
28. Szczypiński PM, Strzelecki M, Materka A, Klepaczko, A. MaZda--a software package for image texture analysis. Comput Methods Programs Biomed 2009; 94:66–76. [CrossRef]
29. Strzelecki M, Szczypinski P, Materka, A. et al. A software tool for automatic classification and segmentation of 2D/3D medical images. Nucl Instrum Meth A 2013; 702:137–140. [CrossRef]
30. Nilsson H, Blomqvist L, Douglas L, et al. Gd-EOB-DTPA-enhanced MRI for the assessment of liver function and volume in liver cirrhosis. Br J Radiol 2013; 86:20120653. [CrossRef]
31. Dai Y, Zeng M, Li R, et al. Improving detection of siderotic nodules in cirrhotic liver with a multi-breath-hold susceptibility-weighted imaging technique. J Magn Reson Imaging 2011; 34:318–325. [CrossRef]
32. Du YP, Jin Z, Hu Y, Tanabe J. Multi-echo acquisition of MR angiography and venography of the brain at 3 Tesla. J Magn Reson Imaing 2009; 30:449–454. [CrossRef]
33. Bülow R, Mensel B, Meffert P, Hernando D, Evert M, Kuehn JP. Diffusion-weighted magnetic resonance imaging for staging liver fibrosis is less reliable in the presence of fat and iron. Eur Radiol 2013; 23:1281–1287. [CrossRef]
34. Leiner T, Kucharczyk W. NSF prevention in clinical practice: summary of recommendations and guidelines in the United States, Canada, and Europe. J Magn Reson Imaging 2009; 30:1357–1363. [CrossRef]